A delivery system targeting bone formation surfaces to facilitate RNAi-based anabolic therapy

Ge Zhang[1,13], Baosheng Guo[1,13], Heng Wu[1,13], Tao Tang[1,13], Bao-Ting Zhang[1,2,13], Lizhen Zheng[1], Yixin He[1], Zhijun Yang[3], Xiaohua Pan[4], Heelum Chow[5], Kinwah To[5], Yaping Li[6], Dahu Li[7], Xinluan Wang[1], Yixiang Wang[8], Kwongman Lee[9], Zhibo Hou[10], Nan Dong[11], Gang Li[1], Kwoksui Leung[1], Leungkim Hung[1], Fuchu He[7], Lingqiang Zhang[7] & Ling Qin[1,12]

Metabolic skeletal disorders associated with impaired bone formation are a major clinical challenge. One approach to treat these defects is to silence bone-formation–inhibitory genes by small interference RNAs (siRNAs) in osteogenic-lineage cells that occupy the niche surrounding the bone-formation surfaces. We developed a targeting system involving dioleoyl trimethylammonium propane (DOTAP)-based cationic liposomes attached to six repetitive sequences of aspartate, serine, serine ((AspSerSer)$_6$) for delivering siRNAs specifically to bone-formation surfaces. Using this system, we encapsulated an osteogenic siRNA that targets casein kinase-2 interacting protein-1 (encoded by *Plekho1*, also known as *Plekho1*). *In vivo* systemic delivery of *Plekho1* siRNA in rats using our system resulted in the selective enrichment of the siRNAs in osteogenic cells and the subsequent depletion of *Plekho1*. A bioimaging analysis further showed that this approach markedly promoted bone formation, enhanced the bone micro-architecture and increased the bone mass in both healthy and osteoporotic rats. These results indicate (AspSerSer)$_6$-liposome as a promising targeted delivery system for RNA interference–based bone anabolic therapy.

Impaired bone formation occurs in several varieties of dysfunctional bone homeostasis. To date, intermittent injection of recombinant human parathyroid hormone (iPTH) is the only bone anabolic agent clinically approved for stimulating bone formation in severe osteoporosis[1,2]. However, iPTH treatment is limited to a 2-y period because of increasing bone resorption over bone formation and a potential risk of developing osteosarcoma in patients receiving iPTH

treatment[3–5]. This limitation has provided an incentive to search for new, safe bone anabolic drugs that do not activate bone resorption.

RNA interference (RNAi), a natural cellular process that regulates gene expression through a highly precise mechanism of sequence-directed gene silencing, could theoretically be used to target any disease-associated pathogenic gene of interest[6]. Accordingly, RNAi-based therapies targeting those genes that have been identified to negatively regulate bone formation without modulating bone resorption could facilitate translational therapy for treating diseases marked by impaired bone formation[7]. However, there is a major concern that the large therapeutic doses of systemically administered siRNA that would be needed to stimulate sufficient bone formation may carry a high risk for adverse effects in nonskeletal tissues[8]. This concern leaves the field with a great challenge when considering the use of these treatments[6]. Thus, development of a specific delivery system for RNAi-based therapies that addresses this issue is highly desirable.

The niche surrounding the bone-formation surfaces is predominantly occupied by osteogenic-lineage cells at various stages of differentiation[3]. All of these cells could be potential targets of pro-osteogenic siRNAs. A practical strategy, then, is to develop a generalized siRNA delivery system that selectively targets bone-formation surfaces to facilitate the delivery of therapeutic siRNAs to the majority of the osteogenic-lineage cells. Such a delivery system would probably allow for a highly targeted dose of therapeutic siRNA to be delivered to the bone while avoiding possible negative side effects to nonskeletal tissues, thus increasing the efficacy and safety of RNAi-based bone anabolic therapy.

To date, two types of stable bone-targeting molecules, bisphosphonates and oligopeptides, have been used to target bone after they have been coupled to nonspecific bone therapeutic agents[9].

[1]Musculoskeletal Research Laboratory, Department of Orthopaedics & Traumatology, The Chinese University of Hong Kong, Hong Kong, China. [2]School of Chinese Medicine, The Chinese University of Hong Kong, Hong Kong, China. [3]School of Chinese Medicine, Hong Kong Baptist University, Hong Kong, China. [4]Department of Orthopedics, Second Hospital of Medical College of Ji Nan University, Shenzhen People's Hospital, Shenzhen, China. [5]School of Pharmacy, The Chinese University of Hong Kong, Hong Kong, China. [6]Center of Drug Delivery System, Shanghai Institute of Materia Medica, Shanghai, Chinese Academy of Sciences, Shanghai, China. [7]State Key Laboratory of Proteomics, Beijing Proteome Research Center, Beijing Institute of Radiation Medicine, Beijing, China. [8]Department of Imaging and Interventional Radiology, The Chinese University of Hong Kong, Hong Kong, China. [9]Lee Hysan Clinical Research Laboratory, The Chinese University of Hong Kong, Hong Kong, China. [10]Biomedical Research and Development Center, Guangdong Provincial Key Laboratory of Bioengineering Medicine, National Engineering Research Center of Genetic Medicine, Jinan University, Guangzhou, China. [11]Institute of Molecular Biology, Nan Kai University, Tianjin, China. [12]Translational Medicine Research & Development Center, Institute of Biomedical and Health Engineering, Shenzhen Institute of Advanced Technology, Shenzhen, China. [13]These authors contributed equally to this work. Correspondence should be addressed to L.Q. (lingqin@cuhk.edu.hk), L.Zhang (zhanglq@nic.bmi.ac.cn) or G.Z. (zhangge@ort.cuhk.edu.hk).

Eight repeating sequences of aspartate (Asp_8), one of the representative targeting oligopeptides, has been reported to preferentially bind to bone-resorption surfaces, whereas alendronate, one of the representative bisphosphonates, is distributed to both bone-formation surfaces and bone-resorption surfaces[10]. However, there remains a lack of bone-targeted molecules that have high selectivity for bone-formation surfaces over bone-resorption surfaces.

The physical chemistry of bone-formation surfaces covered with osteoblasts is characterized by lowly crystallized hydroxyapatite, as well as amorphous calcium phosphonate, whereas the physical chemistry of bone-resorption surfaces covered with osteoclasts is characterized by highly crystallized hydroxyapatite[10]. The stronger affinity of Asp_8 to highly crystallized hydroxyapatite rather than lowly crystallized hydroxyapatite *in vitro* provides an explanation for the preferential binding of Asp_8 to bone-resorption surfaces. Recently, $(AspSerSer)_6$ was found to favorably bind to mantle dentin, which consists of small and randomly oriented crystals, rather than the enamel surface, which consists of elongated and well-oriented hydroxyapatite crystals[11]. Therefore, we postulated that these different bindings of $(AspSerSer)_6$ might depend on the crystallinity of hydroxyapatite. In addition, $(AspSerSer)_6$ also showed favorable binding to osteoblast-mediated mineralizing nodules and amorphous calcium phosphate *in vitro*, implying its potential as a selectively targeting moiety for bone-formation surfaces.

Here we confirm that $(AspSerSer)_6$ is a targeting moiety *in vivo* for bone-formation surfaces. Then, we linked $(AspSerSer)_6$ with a DOTAP-based cationic liposome (approved by the US Food and Drug Administration for clinical trials, NCT00059605) that encapsulates an osteogenic siRNA that targets a recently discovered negative regulator (*Plekho1*) of osteogenic lineage activity without modulating bone resorption[12,13]. We examined $(AspSerSer)_6$-liposome with the *Plekho1* siRNA *in vitro* for its physical chemistry and biological characterization. We also performed a series of *in vivo* studies to examine the biological activities of $(AspSerSer)_6$-liposome plus *Plekho1* siRNA for cell-selective delivery, gene knockdown and bone anabolic action in both healthy and osteoporotic rats.

RESULTS

$(AspSerSer)_6$ as a targeting moiety

We compared the differences in the presence of FITC at various bone-formation or bone-resorption surfaces between adult rats injected

Figure 1 Differential occupancy characteristics of $(AspSerSer)_6$ compared to Asp_8 at bone-formation or bone-resorption surfaces in nondecalcified bone sections using a confocal laser scanning microscope. (**a**) Fluorescence micrographs from rats injected with $(AspSerSer)_6$-FITC (top), Asp_8-FITC (middle) or unlinked FITC (bottom). Left, the white arrows point to the bone-formation surfaces labeled with xylenol orange (XO) (red), and the white arrowheads point to bone-resorption surfaces (eroded surface). Middle, the white arrows point at the locally accumulated $(AspSerSer)_6$-FITC (top) or Asp_8-FITC (middle) (green), and the white arrowheads point to bone-resorption surfaces. Right, a merged image of the left and middle images. Co-staining of $(AspSerSer)_6$-FITC and xylenol orange was found (top row). Scale bars, 50 μm. (**b**) Differential distribution of $(AspSerSer)_6$ from Asp_8 in undecalcified bone sections after co-injection. Fluorescence micrographs from rats co-injected with $(AspSerSer)_6$-FITC and Asp_8-rhodamine (top). Left, the white arrows point to $(AspSerSer)_6$-FITC (green) binding sites. Middle, the white arrowheads point to Asp_8-rhodamine (red). Right, a merged image of the left and middle images. Fluorescence micrographs from rats co-injected with unconjugated FITC and rhodamine (bottom). There was no locally accumulated FITC (green, left) or rhodamine (red, middle) seen. Right, a merged image of the left and middle images. Scale bars, 25 μm.

with FITC-labeled $(AspSerSer)_6$ and those injected with FITC-labeled control peptides (Asp_8) after pre-injection of xylenol orange (a red fluorescent calcium-binding dye capable of labeling new bone deposition at bone-formation surfaces)[14]. We found that bone-formation surfaces (labeled with xylenol orange) were largely co-labeled with $(AspSerSer)_6$ (labeled with FITC) in the rats injected with FITC-labeled $(AspSerSer)_6$, whereas we observed very little co-labeling in the rats injected with the FITC-labeled Asp_8 peptides (**Fig. 1a**). Likewise, there was very little staining of the bone-resorption surfaces that had been labeled by injected FITC-labeled $(AspSerSer)_6$, whereas FITC-labeled Asp_8 peptide did show staining at the bone-resorption surfaces (**Fig. 1a**). Similarly, co-injection of both rhodamine-labeled Asp_8 and FITC-labeled $(AspSerSer)_6$ showed little colocalization of Asp_8 and $(AspSerSer)_6$ (**Fig. 1b**). After ruling out nonspecific staining, we did not find that FITC labeled either bone-formation surfaces or bone-resorption surfaces (**Fig. 1a**).

In vitro characterization of the targeted delivery system

We used standard methods in our preparation for linking the $(AspSerSer)_6$ peptide to the DOTAP-based liposomes that encapsulated the *Plekho1* siRNA (**Supplementary Methods** and **Supplementary Fig. 1a**). We confirmed the osteoblast-activity–promoting effect of the identified *Plekho1* siRNA sequence (**Supplementary Table 1** and **Supplementary Fig. 2**).
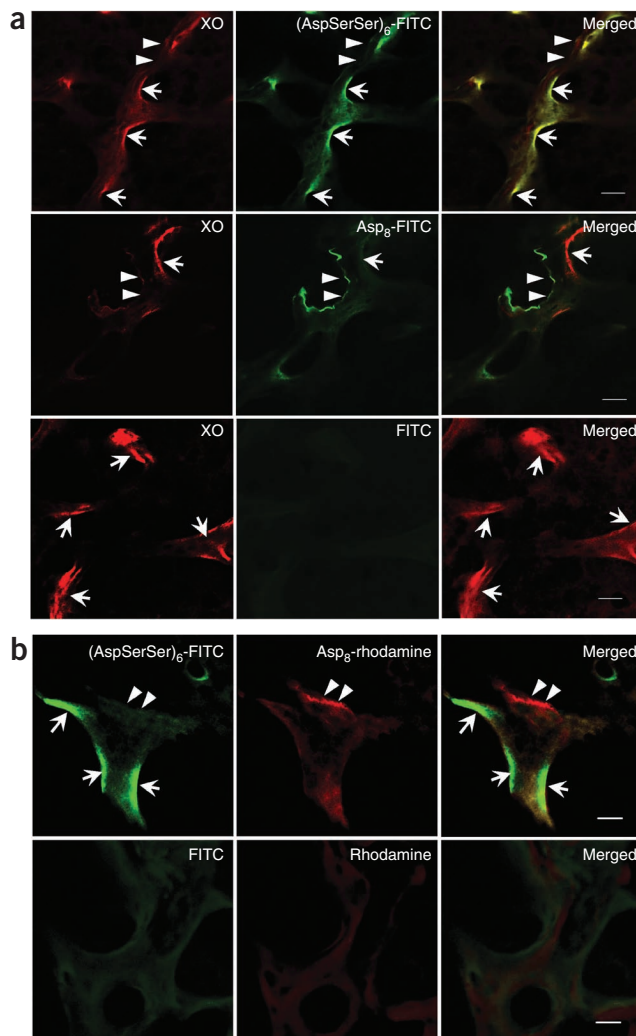
We characterized the physical chemistry of the targeted delivery system in vitro (**Supplementary Results** and **Supplementary Fig. 1b**). The in vitro biological characterization showed that (AspSerSer)$_6$-liposome plus Plekho1 siRNA bound more favorably to lowly crystallized hydroxyapatite than to highly crystallized hydroxyapatite (**Supplementary Table 2** and **Supplementary Fig. 1c**). Further, (AspSerSer)$_6$-liposome prevented the Plekho1 siRNA from serum-mediated degradation (**Supplementary Fig. 1d**) and facilitated the internalization of the linked Plekho1 siRNA in both human osteoblast-like cells (hFOB 1.19 cells) (**Supplementary Fig. 1e**) and human osteoclast-like cells (giant-cell tumors) (data not shown). Functionally, (AspSerSer)$_6$-liposome facilitated Plekho1 gene knockdown in both the hFOB 1.19 cells and giant-cell tumors (**Supplementary Fig. 1f**).

Characterization of the targeted delivery system in vivo

We used biophotonic imaging technology to examine the organ distribution of FAM-labeled Plekho1 siRNA delivered by the liposome with or without the (AspSerSer)$_6$ moiety or delivered as free siRNA without any transfection reagent in 6-month-old female healthy Sprague Dawley rats. We used the siRNA delivered by in vivo jetPEI (a commercialized in vivo transfection reagent for nucleic acid) as a positive control. We found that the intensity of the intraosseous fluorescence signal was strongest in the rats injected with (AspSerSer)$_6$-liposome plus Plekho1 siRNA among all the groups (**Fig. 2a**). However, the intensity of the hepatic fluorescence signal was lower in the rats treated with (AspSerSer)$_6$-liposome plus Plekho1 siRNA than in rats treated with Plekho1 siRNA delivered by either in vivo jetPEI or by the liposome without (AspSerSer)$_6$. The fluorescence signal was barely detectable in the heart, spleen, lungs and kidneys of the rats from all of the treatment groups, except for a small signal that was present in the kidney of the rats injected with free siRNA (**Fig. 2a**). Further, the quantification data from the fluorescence microplate readers were also consistent with the findings from the biophotonic imaging (**Fig. 2b**).

We also examined Plekho1 protein and mRNA expression by western blot and real-time PCR analysis, respectively, in bone and nonskeletal organs after administration of Plekho1 siRNA delivered by the liposome with or without the (AspSerSer)$_6$ moiety. In 6-month-old female healthy Sprague Dawley rats, we found that the efficiency of the Plekho1 gene knockdown in bone was significantly higher after treatment with (AspSerSer)$_6$-liposome plus Plekho1 siRNA as compared to the knockdown achieved by treatment with the liposome (without (AspSerSer)$_6$) plus Plekho1 siRNA ($P < 0.05$) (**Fig. 2c,d**). In contrast, the Plekho1 gene knockdown efficiency in nonskeletal organs (for example, the liver and kidney) was significantly lower after
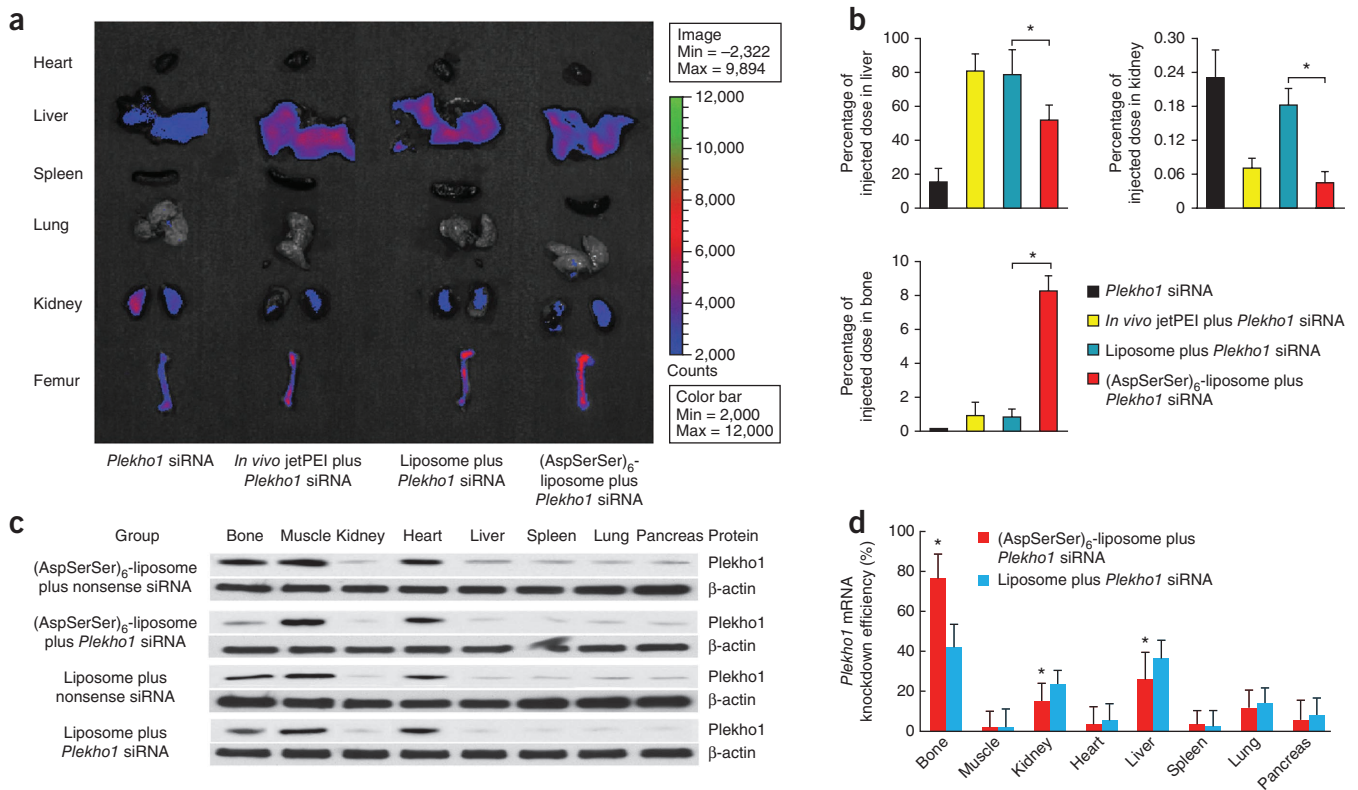
Figure 2 Organ-selective delivery and gene knockdown in vivo. (**a**) Localization of labeled siRNA in rats by a biophotonic-imaging–based analysis after administration of free Plekho1 siRNA, in vivo jetPEI plus Plekho1 siRNA, liposome plus Plekho1 siRNA and (AspSerSer)$_6$-liposome plus Plekho1 siRNA. The intensity of the fluorescence signal was analyzed in isolated hearts, livers, spleens, lungs, kidneys and femurs from the rats. $n = 3$ per group. (**b**) Quantitative analysis by a microplate reader system for the fluorescence of the FAM-labeled siRNA in livers, kidneys and bone tissues after in vivo administration in a separate set of rats using the same delivery systems outlined in **a**. The bone tissues included two sets of femur and tibia samples, as well as vertebra samples. *$P < 0.05$ for comparison with the liposome plus Plekho1 siRNA group by one-way ANOVA with post hoc test. $n = 6$ per group. Data are means ± s.d. (**c**) Representative western blots in various organs for Plekho1 protein after in vivo delivery of Plekho1 siRNA or nonsense siRNA using the indicated methods. β-actin served as an internal control. (**d**) Knockdown efficiency of Plekho1 mRNA expression by a real-time PCR analysis of various organs after in vivo Plekho1 siRNA delivery by the (AspSerSer)$_6$-liposome or liposome methods. Plekho1 knockdown efficiency was calculated by comparing the Plekho1 mRNA expression value in the Plekho1 siRNA group to the knockdown in the nonsense siRNA group. The Plekho1 mRNA expression value was normalized to Gapdh. *$P < 0.05$ for the (AspSerSer)$_6$-liposome plus Plekho1 siRNA group compared to the liposome plus Plekho1 siRNA group. $n = 6$ per group. Data are means ± s.d.

Figure 3 Cell-selective delivery and knockdown efficiency *in vivo*. (**a**) Fluorescence micrographs of cryosections from proximal tibia after injection with free *Plekho1* siRNA (top), liposome plus *Plekho1* siRNA (middle) or (AspSerSer)$_6$-liposome plus *Plekho1* siRNA (bottom) 4 h before the rats were killed. The *Plekho1* siRNA was labeled with FAM (green, left). Immunofluorescence staining was performed to detect Alp-positive osteoblasts (red, middle left). Merged images with DAPI staining showed co-staining of *Plekho1* siRNA and Alp-positive osteoblasts (arrows, yellow, middle right). H&E staining of the same sections is shown (right), and red arrowheads point to bone-formation surfaces, enriched by those cells with pink, which is a merged color of red (osteoblast marker) and blue (DAPI staining for nuclei) in the immunofluorescence staining. Scale bars, 20 μm. (**b**) *Plekho1* knockdown efficiency in Alp-positive cells sorted by FACS after *in vivo* delivery of (AspSerSer)$_6$-liposome plus *Plekho1* siRNA, liposome plus *Plekho1* siRNA or nonsense siRNA linked to liposomes or (AspSerSer)$_6$-liposomes. *Plekho1* mRNA expression was detected by real-time PCR and normalized by glyceraldehyde 3-phosphate dehydrogenase (Gapdh). The *Plekho1* knockdown efficiency was calculated by comparing the *Plekho1* mRNA expression in the *Plekho1* siRNA group to that in the appropriate nonsense siRNA group. Data are means ± s.d. *n* = 6 per group. *$P < 0.05$ (One-way ANOVA with *post hoc* test). NS, no significant difference.
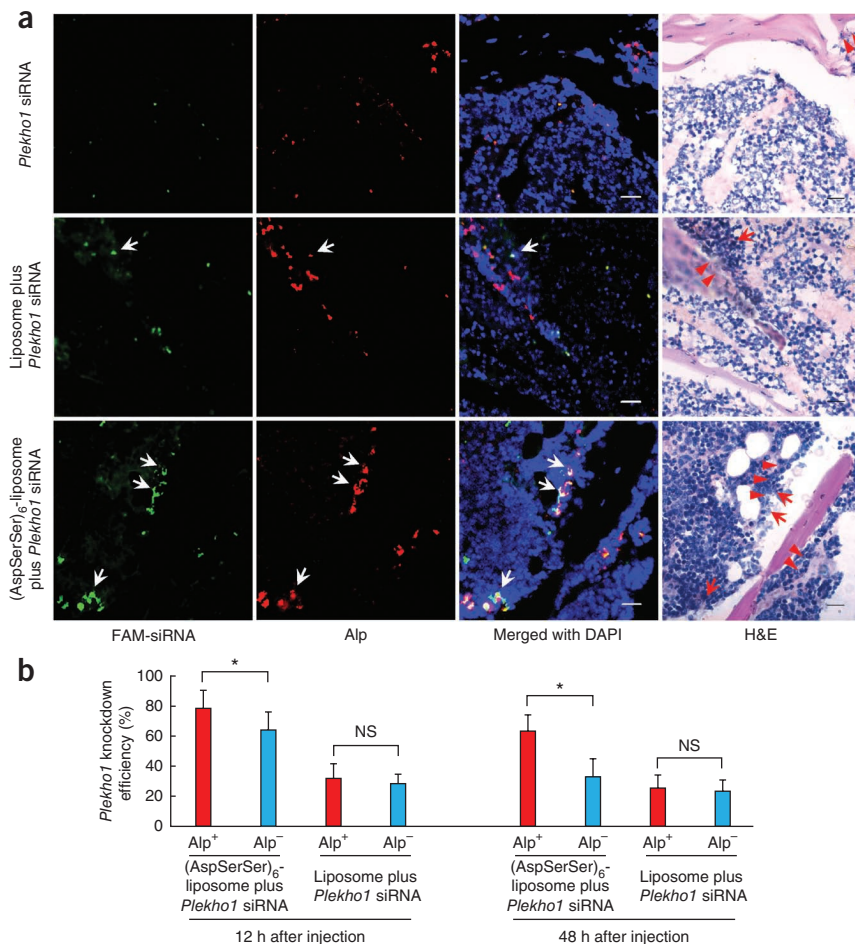
treatment with (AspSerSer)$_6$-liposome plus *Plekho1* siRNA compared to the knockdown efficiency seen after treatment with liposome plus *Plekho1* siRNA ($P < 0.05$) (**Fig. 2c,d**).

In those rats treated with (AspSerSer)$_6$-liposome plus *Plekho1* siRNA, liposome plus *Plekho1* siRNA or *Plekho1* siRNA only, we then immunostained cryosections of the rat proximal tibia and distal femur using markers of osteogenic cells at various differentiation stages, including alkaline phosphatase (Alp), runt-related transcription factor 2 (Runx2), osteocalcin and type I collagen α1 (Col1A1)[15,16]. We found numerous instances of colocalization of the labeled siRNA with Alp-positive (**Fig. 3a**), Runx2-positive (**Supplementary Fig. 3a**), osteocalcin-positive (**Supplementary Fig. 3b**) and Col1A1-positive (**Supplementary Fig. 3c**) cells when we administered (AspSerSer)$_6$-liposome plus *Plekho1* siRNA to the rats, whereas there were few instances of such overlapping staining when we administered liposome plus *Plekho1* siRNA. In addition, the immunohistochemistry for osteoclast-associated receptor (Oscar), a marker specifically expressed in the cell surfaces of pre-osteoclasts and mature osteoclasts[17,18], showed an absence of (AspSerSer)$_6$-liposome plus *Plekho1* siRNA particles in Oscar-positive cells. However, several siRNAs were present in Oscar-positive cells when we administered liposome plus *Plekho1* siRNA to rats (**Supplementary Fig. 3d**).

Further, we examined *Plekho1* mRNA expression in rat bone marrow cells sorted by fluorescence activated cell sorting (FACS) using antibodies to either Alp or Stro-1 (a surface marker on osteoprogenitor cells and pre-osteoblasts)[16]. We found that the *Plekho1* knockdown efficiency in the cells positive for the antibody to Alp was significantly higher than that in either the cells negative for the antibody to Alp ($P < 0.05$) (**Fig. 3b**) or cells positive for an antibody to Oscar ($P < 0.05$) (**Supplementary Fig. 3e**). The *Plekho1* knockdown efficiency in

the cells positive for the antibody to Stro-1 was significantly higher than the knockdown in the cells negative for that antibody at both 12 and 48 h after administration of (AspSerSer)$_6$-liposome plus *Plekho1* siRNA ($P < 0.05$) (**Supplementary Fig. 3f**). In contrast, we found no significant difference in *Plekho1* mRNA expression knockdown efficiency between the cells positive for antibodies to Alp or Stro-1 and the cells negative for these antibodies after administration of liposome plus *Plekho1* siRNA ($P > 0.05$) (**Fig. 3b** and **Supplementary Fig. 3e,f**).

RNAi-mediated bone anabolic action in healthy rats

We used *in vivo* micro computed tomography (microCT) to examine the bone mineral density (BMD) and three-dimensional architecture parameters in trabecular bone of the proximal tibia after the administration of the *Plekho1* siRNA delivered by the liposome with and without the (AspSerSer)$_6$ moiety through tail vein injection in 6-month-old female healthy Sprague-Dawley rats. The statistic analysis by repeated measures analysis of variance (ANOVA) for the *in vivo* microCT data showed that both the 'time effect' and 'time-by-group interaction effect' were statistically significant for all the variables we examined with a statistical significance level at 0.05 (**Supplementary Table 3**). Thus, the data indicate that there was a change over time in the values for all the examined variables and that there were also different change patterns over time among the examined groups of rats. The liposome plus *Plekho1* siRNA group showed a significant increase in BMD, relative bone volume (bone volume/tissue volume), trabecular thickness, trabecular number and connectivity

density (10.01%, 31.91%, 18.82%, 10.04% and 10.56%, respectively) at week 9 after treatment compared to baseline ($P < 0.05$), as well as a significant decrease in structure model index (SMI) (35.07%) at week 9 after treatment compared to baseline ($P < 0.05$). Further, the (AspSerSer)$_6$-liposome plus *Plekho1* siRNA group showed a significant increase from baseline in their BMD, relative bone volume, trabecular thickness, trabecular number and connectivity density (23.12%, 66.87%, 36.37%, 21.65% and 19.18%, respectively) at week 9 after treatment compared to baseline ($P < 0.05$), as well as a significantly larger increase from baseline in these parameters than the group treated with liposome plus *Plekho1* siRNA (13.23%, 27.82%, 15.85%, 12.17% and 12.23%, respectively) at week 9 after treatment ($P < 0.05$). The (AspSerSer)$_6$-liposome plus *Plekho1* siRNA group also showed a significant decrease in trabecular space and SMI (11.61% and 50.00%, respectively) at week 9 compared to baseline ($P < 0.05$), as well as a significant decrease in these two parameters (8.97% and 20.44%, respectively) at week 9 after treatment compared to the liposome plus *Plekho1* siRNA group ($P < 0.05$). However, we found no significant time-course changes from baseline within the 9 weeks of study in all the *in vivo* microCT variables we examined in either the free siRNA group or the age-matched control group (**Fig. 4a**).

Consistent with the microCT quantification data, better organized three-dimensional architecture and a higher bone mass in trabecular bone from the *in vivo* microCT reconstruction images in rats treated with (AspSerSer)$_6$-liposome plus *Plekho1* siRNA compared to rats treated with liposome plus *Plekho1* siRNA, *Plekho1* siRNA alone or PBS (age-matched control) at weeks 6 and 9 after starting the treatment (**Fig. 4b**).

In addition, the bone histomorphometry analysis showed that the mineral apposition rate, bone formation rate, mineralizing surface area, osteoblast surface area and osteoblast number in the group treated with liposome plus *Plekho1* siRNA were all significantly lower than the same parameters in the group treated with (AspSerSer)$_6$-liposome plus *Plekho1* siRNA, but the measures of these parameters in these two groups were remarkably higher than those in the groups treated with free siRNA or PBS or the baseline group; we found no difference in osteoclast surface and osteoclast number among all the groups (**Supplementary Table 4**). We found extensive xylenol and calcein labeling and a larger width between the two labeling bands in the rats treated with (AspSerSer)$_6$-liposome plus *Plekho1* siRNA compared to the rats treated with liposome plus *Plekho1* siRNA, free *Plekho1* siRNA or PBS and compared to the baseline group (**Fig. 4c**).
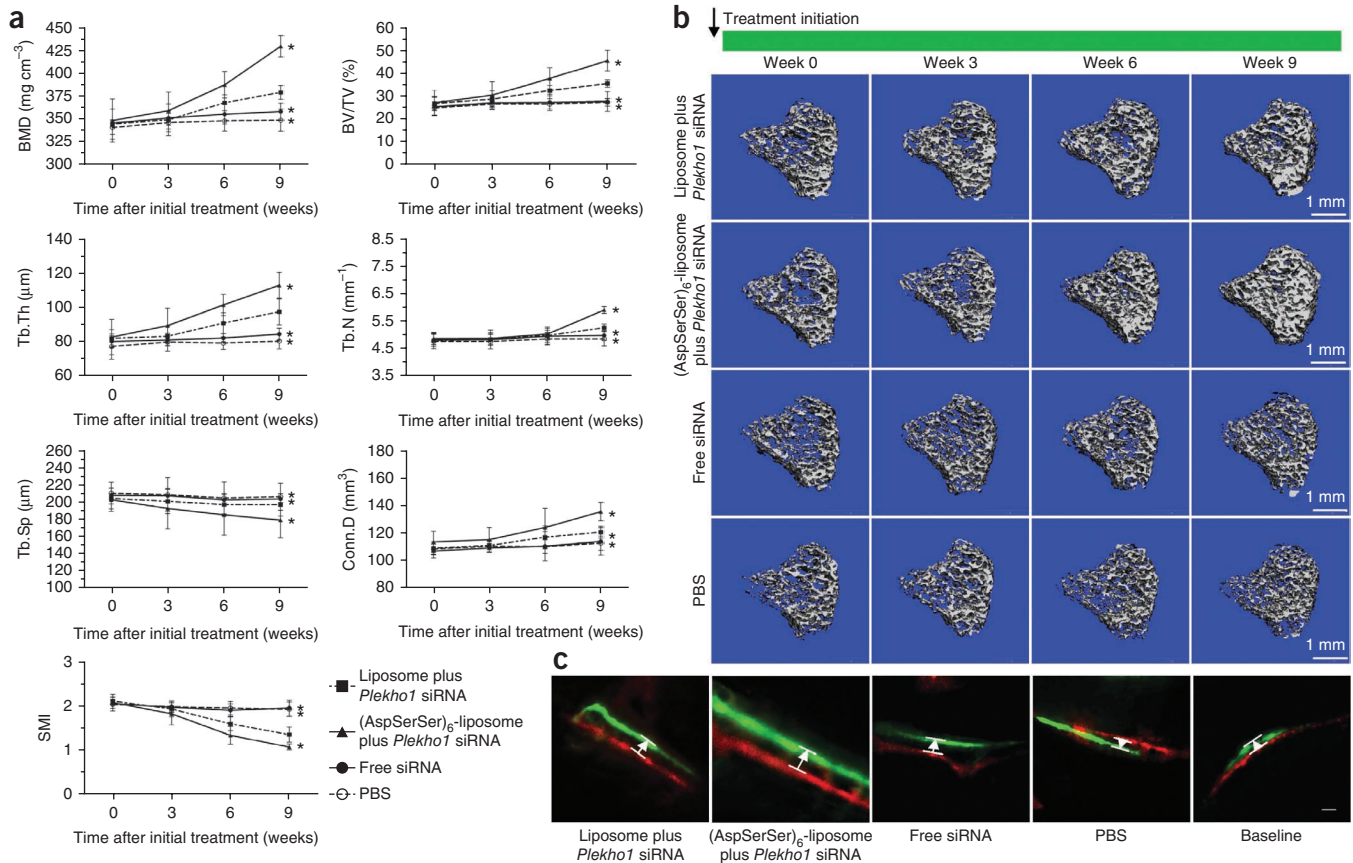

Figure 4 *In vivo* microCT examinations of the three-dimensional trabecular architecture and an *ex vivo* bone formation evaluation in nondecalcified bone sections in healthy rats. (**a**) Plots of the structural parameters (BMD, relative bone volume (BV/TV), trabecular thickness (Tb.Th), trabecular number (Tb.N), connectivity density (Conn.D), structure model index (SMI) and trabecular space (Tb.Sp)) from *in vivo* microCT examination, monitored over time for the four groups of rats examined (rats treated with liposome plus *Plekho1* siRNA, (AspSerSer)$_6$-liposome plus *Plekho1* siRNA, free siRNA or PBS). *$P < 0.05$ compared to the liposome *Plekho1* siRNA group at week 9 after treatment. (**b**) Representative three-dimensional trabecular architecture at the proximal tibia from the respective groups (rats treated with liposome plus *Plekho1* siRNA, (AspSerSer)$_6$-liposome plus *Plekho1* siRNA, free siRNA or PBS) obtained by *in vivo* microCT examination at baseline and at weeks 3, 6 and 9 after treatment. (**c**) Bone formation was examined by sequential labels with fluorescent dye in nondecalcified bone sections from healthy rats. Representative fluorescent micrographs of the trabecular bone sections showed the xylenol (red) and calcein (green) labels in the baseline group and the groups treated with liposome plus *Plekho1* siRNA, (AspSerSer)$_6$-liposome plus *Plekho1* siRNA, free siRNA or PBS. Arrows indicate the space between the xylenol and calcein labeling. Scale bars, 10 μm.
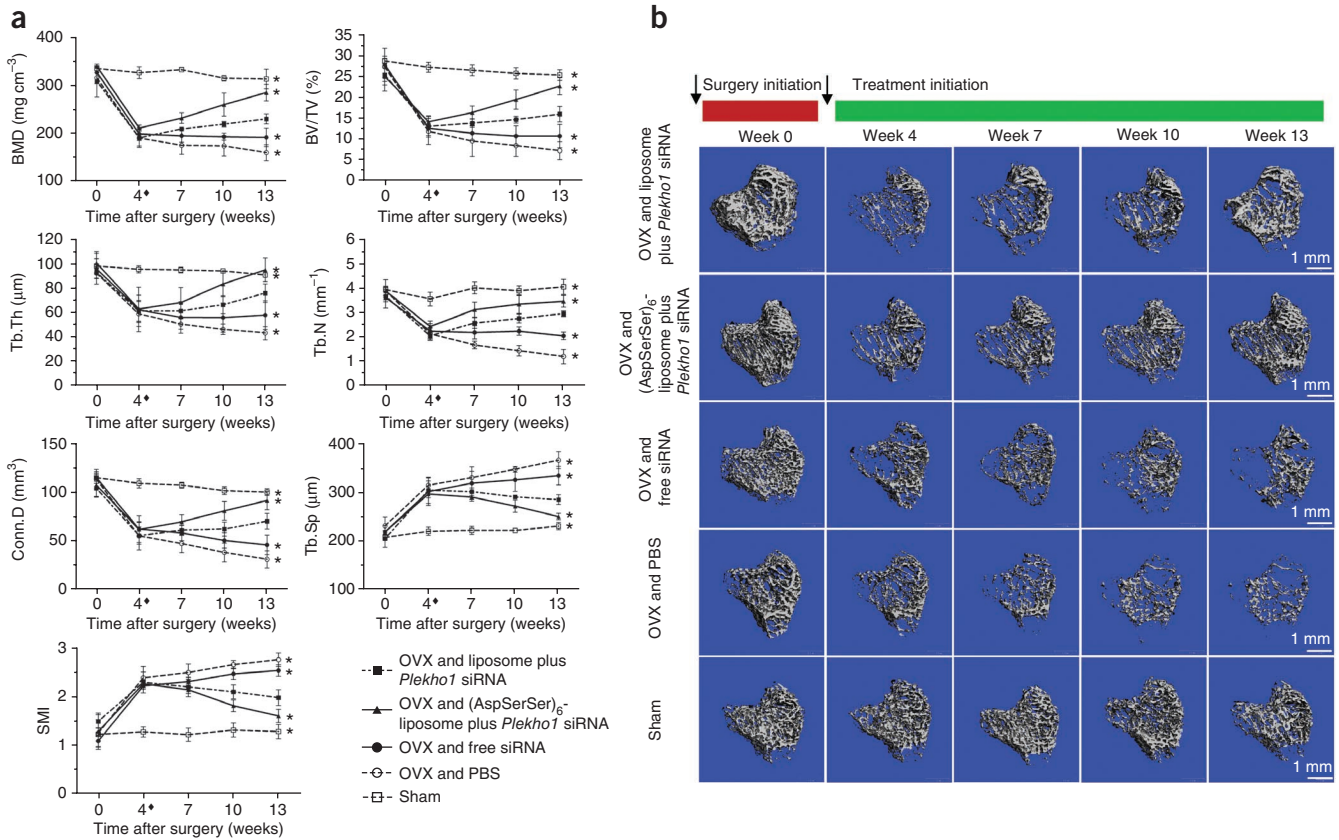
Figure 5 *In vivo* microCT examination of the three-dimensional trabecular architecture in OVX-treated rats. (**a**) Plots of the structural parameters (BMD, relative bone volume (BV/TV), trabecular thickness (Tb.Th), trabecular number (Tb.N), connectivity density (Conn.D), structure model index (SMI) and trabecular space (Tb.Sp)) from an *in vivo* microCT examination, monitored over time for the rats from the sham-treated group and the groups treated with OVX and PBS, OVX and free siRNA, OVX and liposome plus *Plekho1* siRNA and OVX and (AspSerSer)$_6$-liposome plus *Plekho1* siRNA. The repeated measures ANOVA analysis for the *in vivo* microCT data showed that both the time effect and the time-by-group interaction effect were statistically significant for all the examined parameters. *$P < 0.05$ compared to the liposome plus *Plekho1* siRNA group at week 13 after treatment. The diamond indicates the initiation of treatment. (**b**) Representative three-dimensional trabecular architecture at the proximal tibia from the respective groups (sham-treated rats and rats treated with OVX and PBS, OVX and free siRNA, OVX and liposome plus *Plekho1* siRNA, and OVX and (AspSerSer)$_6$-liposome plus *Plekho1* siRNA) obtained by *in vivo* microCT examination at weeks 0, 4, 7, 10 and 13 after OVX.

The quantification of the distance between the xylenol and calcein labeling was also reflected in the bone-formation–related parameters (that is, the mineral apposition rate, bone formation rate, mineralizing surface and osteoblast surface).

RNAi-mediated bone anabolic action in osteoporotic rats

We also used *in vivo* microCT to examine the BMD and three-dimensional architecture parameters in trabecular bone of the proximal tibia after the administration of the *Plekho1* siRNA delivered by the liposome with and without the (AspSerSer)$_6$ moiety in 6-month-old female Sprague-Dawley rats with established osteoporosis induced by ovariectomy (OVX). We initiated the siRNA treatment by tail vein injection at 4 weeks after OVX. The statistical analysis by repeated measures ANOVA for the *in vivo* microCT data (**Supplementary Results**) showed that both the time effect and time-by-group interaction effect were statistically significant with a statistical significance level at 0.05 for all the variables we examined (BMD, relative bone volume, trabecular thickness, trabecular number, trabecular space, connectivity density and SMI); the data also indicated a change over time in the examined variables and different change patterns over time between the examined groups after the administration of treatment (**Fig. 5a**). Briefly, all the above *in vivo* microCT parameters in the group treated with OVX and (AspSerSer)$_6$-liposome plus *Plekho1*

siRNA were almost restored to the pre-surgery values after 9-week treatment (at week 13 after surgery), whereas we did not observe such restoration observed in the group treated with OVX and liposome plus *Plekho1* siRNA within the 9-week siRNA treatment period. Consistently, we found better organized microarchitecture and a higher bone mass in trabecular bone in rats treated with OVX and (AspSerSer)$_6$-liposome plus *Plekho1* siRNA compared to rats treated with OVX and liposome plus *Plekho1* siRNA, free siRNA or PBS (age-matched control) after 6-week treatment and 9-week treatment. (at week 10 and 13 after surgery) (**Fig. 5b**).

DISCUSSION

Currently, there is no available bone-specific targeting delivery system used for siRNA delivery in bone metabolic disorders. Here we designed a siRNA delivery system to specifically target bone-formation surfaces and, thus, facilitate the delivery of therapeutic cargos to the osteogenic-lineage cells. This delivery system could establish the foundation for translating RNAi-based therapies from basic science to clinic applications in the musculoskeletal field.

In our *in vitro* studies described here, we find that (AspSerSer)$_6$ has a higher binding affinity to lowly crystallized hydroxyapatite (similar to what is found at the bone-formation surface) than to highly crystallized hydroxyapatite (similar to what is found at the bone-resorption

surface)[19], implying that this moiety has the potential to selectively bind to bone-formation surfaces rather than bone-resorption surfaces. Furthermore, in our *in vivo* studies that included dynamic bone histomorphometry, we found that (AspSerSer)$_6$ favorably binds to bone-formation surfaces rather than bone-resorption surfaces, the mechanism for which is related to the chemical biology that is involved in the interaction between (AspSerSer)$_6$ and crystallized hydroxyapatite (**Supplementary Discussion**)[4,9,14,20–24].

The data from both the biophotonic imaging and microplate reader systems consistently suggested that (AspSerSer)$_6$-liposome could facilitate the delivery of the linked siRNA to bone (with an approximately tenfold more siRNA delivered to the bone in rats treated with (AspSerSer)$_6$-liposome plus *Plekho1* siRNA than that seen in rats treated with liposome plus *Plekho1* siRNA) and reduce its delivery to nonskeletal organs. To date, there have been no reports of bone-targeting delivery systems for RNAi-based therapy. Furthermore, real-time PCR and western blot analyses in our study consistently suggested that (AspSerSer)$_6$-liposome could facilitate RNAi-based gene knockdown in a bone-selective manner.

The immunohistochemistry data indicated that (AspSerSer)$_6$-liposome could facilitate the delivery of siRNA to osteogenic cells at various differentiation stages. Thus, we did flow cytometry and found that (AspSerSer)$_6$-liposome plus *Plekho1* siRNAs, unlike liposome plus *Plekho1* siRNAs, facilitate RNAi-based gene knockdown in osteogenic cells at various stages of differentiation but, notably, not in osteoclastic cells. We observed that this exclusion of the knockdown of *Plekho1* that was mediated by (AspSerSer)$_6$-liposome plus *Plekho1* siRNA in osteoclasts *in vivo* was not present *in vitro*, where we found a similar knockdown efficiency facilitated by the (AspSerSer)$_6$-liposome plus *Plekho1* siRNA in both human osteoblast-like cells and human osteoclast-like cells. This inconsistency could be explained by the lack of a skeletal domain in the cell culture we used and the existence of this domain in the *in vivo* animal studies. The mechanism of the cell-specific delivery for siRNA is postulated to involve the increased interaction between *Plekho1* siRNA and the osteogenic cells, as facilitated by (AspSerSer)$_6$ (**Supplementary Discussion** and **Supplementary Fig. 4**).

The flexible extravasation of the (AspSerSer)$_6$-liposome plus *Plekho1* siRNA into bone fluid and the increased cellular internalization of the linked siRNA induced by the (AspSerSer)$_6$-liposome platform are also reflected in the present study (**Supplementary Discussion**)[25–27].

The bone histomorphometry data from the healthy rats indicated that the targeting moiety (AspSerSer)$_6$ was able to facilitate the functional longevity and activity of osteoblasts after it facilitated *Plekho1* gene silencing that was mediated by liposome plus *Plekho1* siRNA. Further, the *in vivo* microCT data from the healthy rats indicated that the targeting moiety (AspSerSer)$_6$ could significantly facilitate increased bone mass and an improved trabecular architecture. It is known that iPTH stimulates both bone-forming and bone-resorbing cells, which complicates its clinical use[2,28]. In contrast, bone resorption was not activated by (AspSerSer)$_6$-liposome plus *Plekho1* siRNA. Notably, our *in vivo* microCT data from the osteoporotic rats indicated that the targeting moiety (AspSerSer)$_6$ could also significantly facilitate a liposome plus *Plekho1* siRNA–mediated increase in bone mass and an improvement in the trabecular architecture to the pre-surgery values at week 9 after treatment, whereas treatment with liposome plus *Plekho1* siRNA did not restore these values to their pre-surgery levels. Taken together, these data suggest that the targeting moiety (AspSerSer)$_6$ can facilitate improvements in bone anabolic action mediated by liposome plus *Plekho1* siRNA in both healthy rats and osteoporotic rats.

In summary, (AspSerSer)$_6$-liposome is a promising targeting system for specifically delivering siRNA drugs to bone-formation surfaces and the osteogenic cells that reside there, thus providing a potential solution to the bottleneck in clinical translation of RNAi-based bone anabolic therapies.

METHODS
Methods and any associated references are available in the online version of the paper at http://www.nature.com/naturemedicine/.

Note: Supplementary information is available on the Nature Medicine website.

1. Black, D.M. *et al*. The effects of parathyroid hormone and alendronate alone or in combination in postmenopausal osteoporosis. *N. Engl. J. Med.* **349**, 1207–1215 (2003).
2. Hodsman, A.B. *et al*. Parathyroid hormone and teriparatide for the treatment of osteoporosis: a review of the evidence and suggested guidelines for its use. *Endocr. Rev.* **26**, 688–703 (2005).
3. Cosman, F. *et al*. Daily and cyclic parathyroid hormone in women receiving alendronate. *N. Engl. J. Med.* **353**, 566–575 (2005).
4. Lindsay, R. *et al*. Randomised controlled study of effect of parathyroid hormone on vertebral-bone mass and fracture incidence among postmenopausal women on oestrogen with osteoporosis. *Lancet* **350**, 550–555 (1997).
5. Neer, R.M. *et al*. Effect of parathyroid hormone (1–34) on fractures and bone mineral density in postmenopausal women with osteoporosis. *N. Engl. J. Med.* **344**, 1434–1441 (2001).
6. López-Fraga, M., Martinez, T. & Jimenez, A. RNA interference technologies and therapeutics: from basic research to products. *BioDrugs* **23**, 305–332 (2009).
7. Novina, C.D. & Sharp, P.A. The RNAi revolution. *Nature* **430**, 161–164 (2004).
8. Itaka, K. *et al*. Bone regeneration by regulated *in vivo* gene transfer using biocompatible polyplex nanomicelles. *Mol. Ther.* **15**, 1655–1662 (2007).
9. Wang, D., Miller, S.C., Kopeckova, P. & Kopecek, J. Bone-targeting macromolecular therapeutics. *Adv. Drug Deliv. Rev.* **57**, 1049–1076 (2005).
10. Wang, D. *et al*. Osteotropic peptide that differentiates functional domains of the skeleton. *Bioconjug. Chem.* **18**, 1375–1378 (2007).
11. Yarbrough, D.K. *et al*. Specific binding and mineralization of calcified surfaces by small peptides. *Calcif. Tissue Int.* **86**, 58–66 (2010).

12. Lu, K. *et al.* Targeting WW domains linker of HECT-type ubiquitin ligase Smurf1 for activation by *Ckip-1*. *Nat. Cell Biol.* **10**, 994–1002 (2008).
13. Zhang, L. *et al.* The PH domain containing protein *Ckip-1* binds to IFP35 and Nmi and is involved in cytokine signaling. *Cell. Signal.* **19**, 932–944 (2007).
14. Stuart, A.J. & Smith, D.A. Use of the fluorochromes xylenol orange, calcein green, and tetracycline to document bone deposition and remodeling in healing fractures in chickens. *Avian Dis.* **36**, 447–449 (1992).
15. Aubin, J. & JNM., H. Bone cell biology: osteoblast, osteocyte and osteoclasts. in *Pediatric Bone* 43–47 (Academic Press, San Diego, California, USA, 2002).
16. Gronthos, S. *et al.* Differential cell surface expression of the STRO-1 and alkaline phosphatase antigens on discrete developmental stages in primary cultures of human bone cells. *J. Bone Miner. Res.* **14**, 47–56 (1999).
17. Ishikawa, S. *et al.* Involvement of FcRγ in signal transduction of osteoclast-associated receptor (OSCAR). *Int. Immunol.* **16**, 1019–1025 (2004).
18. Kim, N., Takami, M., Rho, J., Josien, R. & Choi, Y. A novel member of the leukocyte receptor complex regulates osteoclast differentiation. *J. Exp. Med.* **195**, 201–209 (2002).
19. Posner, A.S. & Betts, F. Synthetic amorphous calcium-phosphate and its relation to bone-mineral structure. *Acc. Chem. Res.* **8**, 273–281 (1975).
20. Hoang, Q.Q., Sicheri, F., Howard, A.J. & Yang, D.S. Bone recognition mechanism of porcine osteocalcin from crystal structure. *Nature* **425**, 977–980 (2003).
21. Midura, R.J. *et al.* Bone acidic glycoprotein-75 delineates the extracellular sites of future bone sialoprotein accumulation and apatite nucleation in osteoblastic cultures. *J. Biol. Chem.* **279**, 25464–25473 (2004).
22. Steitz, S.A. *et al.* Osteopontin inhibits mineral deposition and promotes regression of ectopic calcification. *Am. J. Pathol.* **161**, 2035–2046 (2002).
23. Takahashi-Nishioka, T. *et al.* Targeted drug delivery to bone: pharmacokinetic and pharmacological properties of acidic oligopeptide-tagged drugs. *Curr. Drug Discov. Technol.* **5**, 39–48 (2008).
24. Wang, D., Miller, S., Sima, M., Kopeckova, P. & Kopecek, J. Synthesis and evaluation of water-soluble polymeric bone-targeted drug delivery systems. *Bioconjug. Chem.* **14**, 853–859 (2003).
25. Federman, N. & Denny, C.T. Targeting liposomes toward novel pediatric anticancer therapeutics. *Pediatr. Res.* **67**, 514–519 (2010).
26. Wang, G., Kucharski, C., Lin, X. & Uludag, H. Bisphosphonate-coated BSA nanoparticles lack bone targeting after systemic administration. *J. Drug Target.* **18**, 611–626 (2010).
27. Cullis, P.R., Mayer, L.D., Bally, M.B., Madden, T.D. & Hope, M.J. Generating and loading of liposomal systems for drug-delivery applications. *Adv. Drug Deliv. Rev.* **3**, 267–282 (1989).
28. Vegni, F.E., Corradini, C. & Privitera, G. Effects of parathyroid hormone and alendronate alone or in combination in osteoporosis. *N. Engl. J. Med.* **350**, 189–192, author reply 189–192 (2004).

ONLINE METHODS

Study profile. We prepared the $(AspSerSer)_6$-liposome plus *Plekho1* siRNA after examination of the nature of $(AspSerSer)_6$ and *Plekho1* siRNA (pre-study work 3). After those examinations, eight specific studies were performed, including 'study 1' for physical chemistry characterization *in vitro*, 'study 2' for binding affinity to hydroxyapatite and resistance against serum-mediated degradation *in vitro*, 'study 3' for cellular internalization and knockdown efficiency *in vitro*, 'study 4' for organ-selective delivery *in vivo*, 'study 5' for organ-specific gene knockdown *in vivo*, 'study 6'

for tissue- or cell-selective delivery *in vivo*, 'study 7' for cell-selective gene knockdown *in vivo* and 'study 8' for bone anabolic action *in vivo*. Details are provided in the **Supplementary Methods**. The procedures described in the above studies were approved by Animal Experimentation Ethics Committee of The Chinese University of Hong Kong (ref. no. 09/072/MIS).

Additional methods. Detailed methodology is described in the **Supplementary Methods**.